A method for the seismic design of multi-propped retaining walls

Luigi Callisto
Professor, University of Rome La Sapienza
Dept of Structural and Geotechnical Engineering
Via Eudossiana 18
00184 - Roma
luigi.callisto@uniroma1.it

ABSTRACT

This paper describes and validates a novel method for the seismic design of multi-propped retaining walls. The method is conceived as an application to excavations of the static-non-linear analysis employed for structural systems: this is a decoupled method, whereby the seismic demand and the seismic capacity are derived independently and are subsequently compared onto the acceleration-displacement plane. The seismic demand is described by an elastic response spectrum, that can be either derived from a ground response analysis, or can be directly specified by a building code. Conversely, the seismic capacity is obtained by applying horizontal static forces on the same model used to analyse the static construction sequence. The method is readily applicable in engineering practice, and has the advantage of considering explicitly the following aspects: (i) the influence of the construction sequence on the seismic response of the system; (ii) the deformability of the soil-structure system; (iii) the non-linear behaviour of the soil, including the attainment of its strength during the construction stages and the ensuing earthquake loading.

Keywords

Retaining structures, Earthquake Engineering, Non-linear analysis

1. INTRODUCTION

In the methods currently employed for the seismic design of retaining structures the seismic action is taken to be proportional to the peak ground acceleration (PGA). The current draft of Eurocode 8 part 5 (CEN 2023a) can be taken as a paradigmatic example: although in the new generation Eurocodes (e.g. CEN 2023b) the basic parameter defining the seismic action is the maximum spectral acceleration S_α, the actions on retaining structures are taken proportional to the quantity S_α/F_0, which is in fact the PGA, as F_0 is the maximum amplification coefficient. Similarly, the Italian Building Code (NTC 2018) prescribes that actions on earth retaining structures should be evaluated as a fraction of PGA. Since the PGA is the spectral acceleration at a null vibration period, this way to describe the seismic action contains the implicit assumption that the response of the soil-structure system is rigid-perfectly plastic. While this assumption is useful for studying ultimate conditions, it is not able to describe the actual dynamic response of the system under consideration.

A different class of methods to design earth retaining structures for seismic loading assumes that the soil has a linearly viscous-elastic behaviour, (e.g. Wood 1974, Younan and Veletsos 2000, Branderberg et al. 2015). This methods have the disadvantage of neglecting completely the non-linear behaviour of the soil, including the mobilisation of soil strength during the construction stages and the non-linear response of the system during the earthquake shaking.

The present paper proposes to design multi-propped retaining structure by extending to this class of geotechnical systems the non-linear static (or push-over) analysis commonly employed in the seismic design of structural systems. Specifically, this paper takes the view that in current practice the static design of this type of retaining structures is based very often on numerical models that study the soil-structure interaction, accounting for the construction stages and the non-linear soil behaviour, and proposes to extend these same models to carry out a push-over analyses of the system.

Static non-linear analysis was used by Cecconi et al (2014) to evaluate internal forces in cantilevered embedded retaining wall. More recently, Laguardia et al. (2020) employed a similar approach to study the seismic behaviour of displacing retaining structures. However, since in that case the main objective of the design was the prediction of the

permanent deformation undergone by the system, the elastic response spectrum had to be complemented by information on the number of cycles. On the contrary, multi-propped retaining walls can be regarded as non-displacing retaining structures, in the sense that if the structural members are designed to remain in the elastic range these systems cannot accumulate displacements. Therefore, the seismic design of these structures includes only the evaluation of the maximum instantaneous internal forces in the structural members, and therefore the description of the seismic action provided by an elastic response spectrum may be deemed complete.

2. CASE STUDY

The design method is illustrated with reference to an idealised excavation retained by a couple of embedded retaining walls, that in turn are mutually constrained by two propping levels. Figure 1 shows the geometry of the excavation together with the plane strain finite difference grid used in FLAC2D v.7 Itasca (2011) for the computations presented in this paper (Fortuna 2020). Table I reports the mechanical properties of the structural members, that were modelled as beam elements: the walls are made with 0.5 m diameter reinforced concrete piles with a spacing of 0.7 m, while the propping levels are 0.8 m-thick reinforced concrete slabs. The excavation is carried out in a dry coarse-grained soil. The mechanical behaviour of the soil is described by a non-linearly elastic perfectly plastic model, having a Mohr-Coulomb plasticity criterion. Soil properties are reported in Table II. The shear modulus follows the Seed and Idriss (1979) modulus decay curve: this feature is obtained through a specific routine (written in the FLAC language *fish*) that updates in each grid zone at each calculation step the shear modulus on the basis of the maximum shear strain computed at the previous step.

Table I – Properties of structural elements

Element	Section type	Axial stiffness (kN/m)	Bending stiffness (kN m)	Density per unit length (Mg/m)
Retaining wall	Adjacent piles	8.4×10^6	1.3×10^5	0.7
Propping levels	Concrete slab	2.4×10^7	1.3×10^6	2.0

Table II – Soil properties

γ (kN/m^3)	c' (kPa)	φ' (°)	ψ (°)	δ (°)	ν	G_0/p_{ref}	K_0
20	0	30	0	20	0.3	$1000\left(\frac{p'}{p_{ref}}\right)^{0.5}$	0.5

Legend: γ: unit weight; c': cohesion; φ': angle of shearing resistance; ψ: dilation angle; δ: soil-wall roughness angle; ν: Poisson ratio; G_0: small-strain shear stiffness; p'; mean effective stress; p_{ref} = 100 kPa; K_0 = earth pressure coefficient at rest.

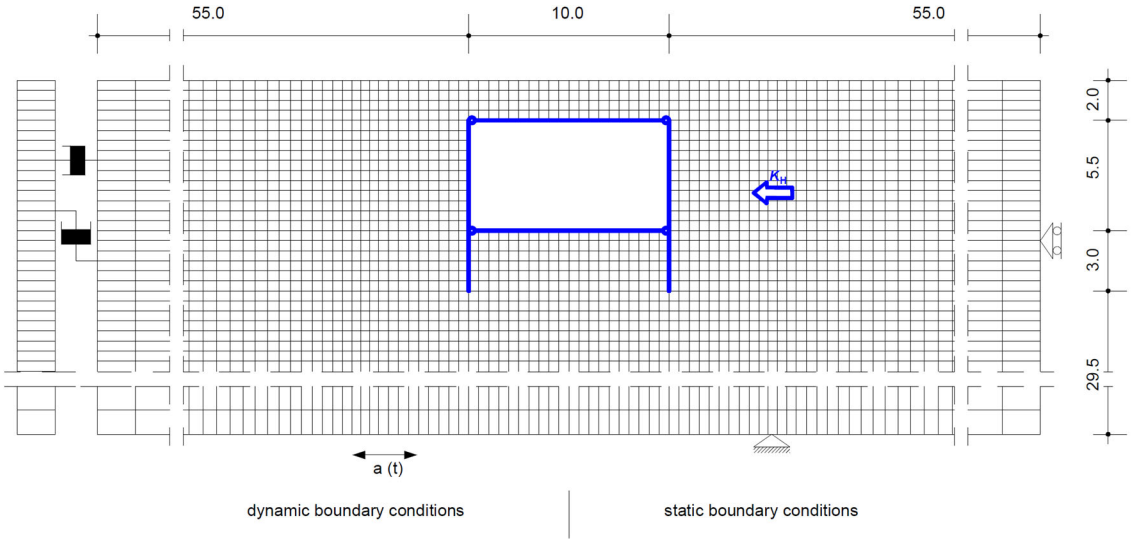

Figure 1 – Layout of the case study and finite-difference grid, with an indication of the different boundary conditions used for the static and the dynamic calculations.

To develop the case study, the construction sequence was simulated first, employing the static boundary conditions depicted in the right side of Figure 1. The construction sequence includes a first 2 m-deep excavation allowing the construction of the first propping level, the placement of the soil fill above this propping level, the completion of the excavation down to the depth of 7.5 m, and finally the construction of the bottom prop level. It is assumed that both props are hinged to the retaining wall.

After the static construction sequence, the finite difference grid was subjected to the base shaking provided by three different horizontal acceleration time histories, namely the Tolmezzo, Arcelik, and L'Aquila records. Figure 2 shows the 5 %-damped elastic response spectra while Table III reports some motion parameters for these records. In the dynamic analyses, these records were applied directly to the bottom nodes of the grid,

neglecting any effect of the bedrock compliance. This is reasonable for the present study, as it is not intended to simulate a real earthquake scenario, but rather to develop an idealised case study for the validation of the simplified design procedure. In the dynamic stage, the boundary conditions at both the lateral sides of the mesh included the FLAC2D free-field boundaries, as depicted in the left side of Figure 1. The same non-linearly elastic, perfectly plastic soil model used for the static simulation was employed, but under dynamic conditions this was obtained by activating the hysteretic damping option in FLAC2D, that uses the Masing unloading-reloading curve to describe energy dissipation. The reader may refer to Itasca (2011) or to Callisto and Soccodato (2010) and Callisto (2014) for further details on the dynamic analyses carried out with FLAC2D.

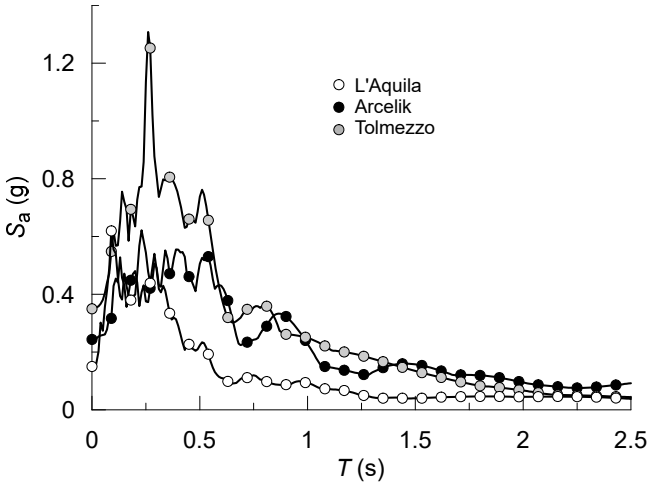

Figure 2 – Elastic response spectra of the acceleration time histories used as seismic actions, plotted for a damping ratio ξ = 5 %.

Table III – Properties of the seismic motions

Record	PGA (g)	I_A (m/s)	$T_{5\text{-}95}$ (s)	T_m (s)
Tolmezzo	0.35	0.80	4.2	0.40
Arcelik	0.24	0.55	7.4	0.70
L'Aquila	0.15	0.40	8.4	0.25

Legend: PGA: peak ground acceleration; I_A; Arias intensity; $T_{5\text{-}95}$; significant duration; T_m: mean quadratic period

3. DEVELOPMENT OF THE DESIGN METHOD

The proposed method is analogous to the Capacity Spectrum Method (Freeman 1998) adopted by several seismic guidelines and codes (e.g. FEMA 440, 2005) for the non-linear static analysis of structures. The method expresses the dynamic response of the structure

through its capacity curve that relates the acceleration to the displacement of the structure. The capacity curve can be evaluated by performing a static push-over analysis of the numerical model, starting from the end of the construction stage and applying horizontal inertial forces to the system. In the present study, the horizontal forces are obtained multiplying the nodal masses by a uniform acceleration $k_H \times g$ that is progressively increased, eventually leading to the collapse of the system. The assumption of spatial uniformity for the acceleration is based on the first vibration mode of the system, which is characterized by a nearly constant spatial distribution of acceleration along the upper third of the soil deposit. This is where most of the soil interacting with the retaining structure is located. (Callisto 2014, Lorusso 2017, Callisto 2023).

The capacity curve obtained for the system of Figure 1 is plotted in Figure 3(b), where the seismic coefficient k_H is plotted against the horizontal displacement of the top of the wall u. At large displacements, the seismic coefficient tends to its the critical values k_C, that for the present case is close to the critical acceleration of the entire soil domain ($k_C = \tan \varphi' = 0.58$). However, as shown by the velocity vectors of Figure 4.a, the plastic mechanism activated under critical conditions is localised around the retaining structure. The deformed grid depicted in Figure 4.b shows that, because the structural elements are designed to remain in the elastic range, most of the displacements are produced by deformation occurring in the soil. As a result, the capacity curve is not particularly sensitive to the specific structural point chosen, and expresses the response to the inertial forces of the soil volume that interacts with the retaining system.

For each value of the seismic coefficient, the push-over analysis provides the distribution of the internal forces in the structural elements: for instance Figure 3(a) shows the seismic increase of the bending moment in the wall at the depth of the lower prop, ΔM_B, as a function of k_H. In the approximate method the internal forces in the structural members can be obtained by comparing the seismic demand and the capacity curve as follows:

- The seismic demand is obtained by performing a one-dimensional ground response analysis, and determining the equivalent accelerogram $a_{eq}(t)$ along the wall, using the procedure proposed by Seed and Martin (1966):

$$a_{eq}(t) = g \frac{\tau_H(t)}{\sigma_{VH}} \tag{1}$$

where $\tau_H(t)$ is the time history of the shear stress computed in the ground response analysis at an elevation equal to the depth of the wall (10.5 m for the present case) and σ_{VH} is the total vertical stress acting at the same depth.

- The response spectrum of the accelerogram is plotted in the AD plane for a given damping ratio ξ (for instance, 5 %) and a first performance point is obtained at the intersection of the spectrum with the capacity curve.

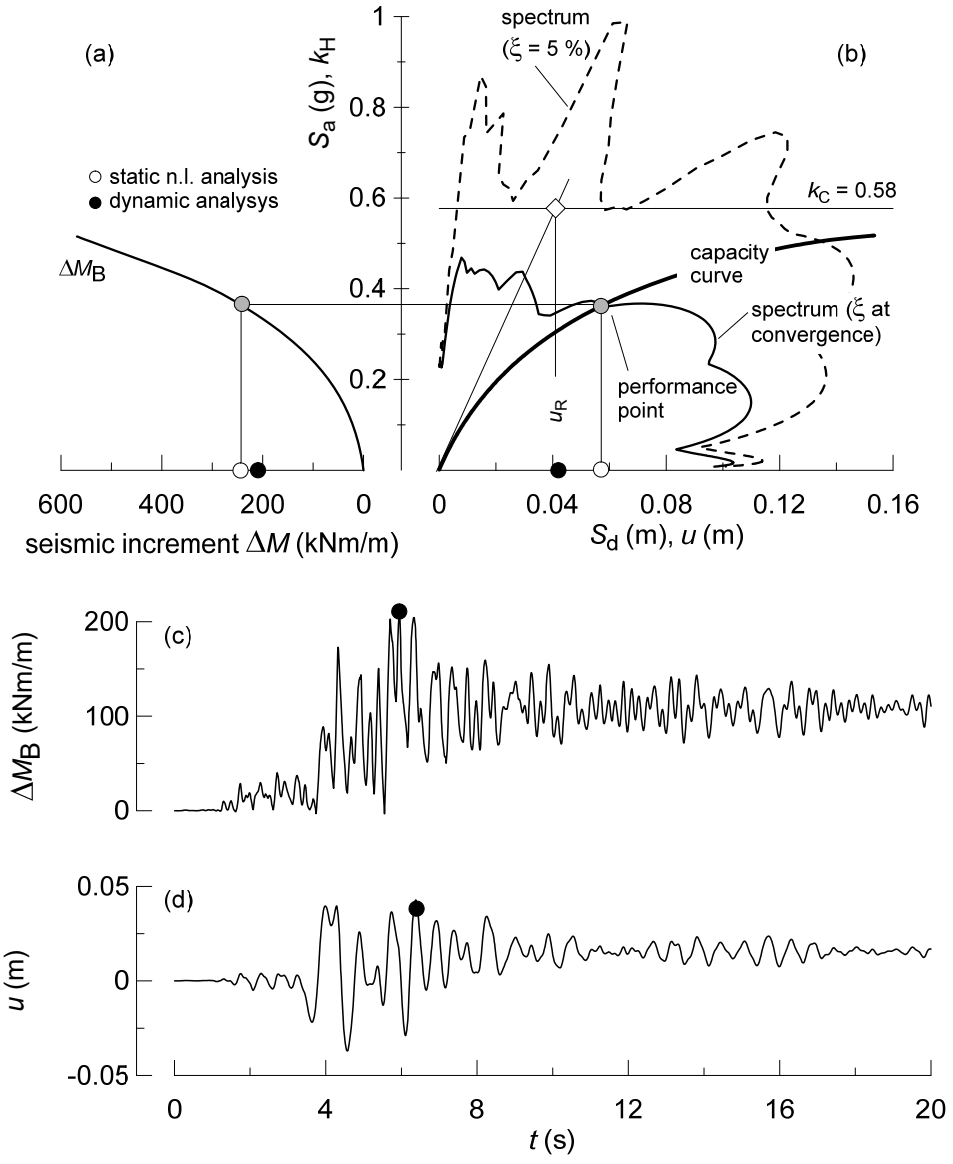

Figure 3 – Tolmezzo record. (a), (b) static push-over analysis: (b) analysis in the AD plane; (a) increment in bending moment obtained from the static push-over analysis. (c), (d) time-histories of the increment in bending moment and of the wall displacement obtained from the dynamic analysis.

- An updated value of ξ is found by assuming that the capacity curve is symmetric, and that the unloading-reloading curve obeys the Masing (1926) criterion. A useful assumption is that the capacity curve can be approximated by a hyperbolic relationship The application of the Masing criterion to the hyperbolic model leads to the following expression for the damping ratio:

$$\xi = \frac{2}{\pi}\left\{2\left(1-\frac{u_R}{u}\right)\left[1-\frac{\ln\left(1+u/u_R\right)}{u/u_R}\right]-1\right\} \tag{2}$$

  where u is the displacement at the performance point and u_R is the reference displacement depicted in Figure 3(b).

- The elastic response spectrum is re-evaluated for this updated damping ratio, and the procedure is iterated until the difference between two subsequent values of ξ becomes smaller of a given tolerance. Usually only two to three iterations are necessary to match a tolerance of 1 %.

- At convergence, the intersection of the elastic response spectrum and the capacity curve provides the maximum instantaneous seismic displacement u and the maximum acceleration $k_H \times g$ for the system. The results of the static push-over analysis provide, for the above acceleration, the distribution of the internal forces in the structural elements.

In the example of Figure 3, relative to the Tolmezzo record, the open symbols indicate the values of u and ΔM_B found from the static push-over analysis (see Figure 5 for the definition of ΔM_B), while the full symbols represent the results of the full dynamic analysis carried out applying the Tolmezzo accelerogram at the base of the soil-structure numerical model. Figures 3(c) and (d) depicts the corresponding time histories of u and ΔM_B. Given the simplicity of the push-over analysis, the agreement of the method with the results of the reference dynamic analysis is remarkably good.

Figure 5 shows the distribution of the bending moments obtained at the end of the excavation phases (labelled as "initial") and, for the Tolmezzo record, the envelopes of the bending moments obtained from the dynamic analyses and using the proposed simplified procedure (static non-linear analysis). For this latter case, the envelope is

obtained considering, for the value of k_H found at the end of the iterations, the distribution of bending moment in the two facing walls. It can be appreciated that the distribution of the bending moments evaluated with the simplified method are in a good agreement with those computed with the full numerical analysis.

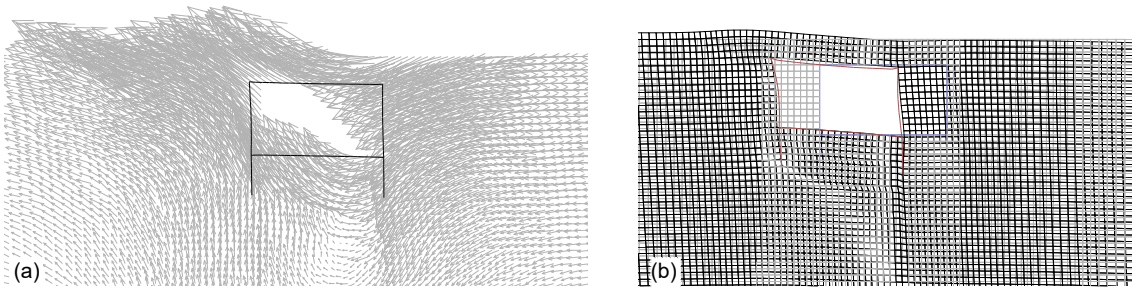

Figure 4 – (a) velocity vectors and (b) deformed grid at the attainment of the critical acceleration.

4. GENERALISATON AND VALIDATION

In the practical application of the method, the seismic demand needs to be derived either from a group of accelerograms, or from a code-specified response spectrum. Therefore, in order to generalise the applicability of the method, the above procedure was applied adopting as the seismic demand the average response spectrum obtained by propagating through a one-dimensional soil column the three accelerograms of Figure 2. In turn, this average spectrum was interpolated using the spectral shape provided by the Italian seismic code. Figure 6 shows the results of the ground response analysis, the average spectrum and the code spectrum used for the interpolation, while Figure 7 depicts the implementation of the method using the code spectrum and referring to the increments of bending moments ΔM_A and ΔM_B computed at the locations show in Figure 5. When using the code spectrum, the dependence of the spectral acceleration and displacement on the damping ratio were evaluated using the expression for the reductive coefficient η reported in both the Italian code and the current Eurocode 8 (CEN 2003):

$$\eta = \sqrt{10/(5+\xi)} \geq 0.55 \tag{3}$$

where ξ is expressed as a percentage.

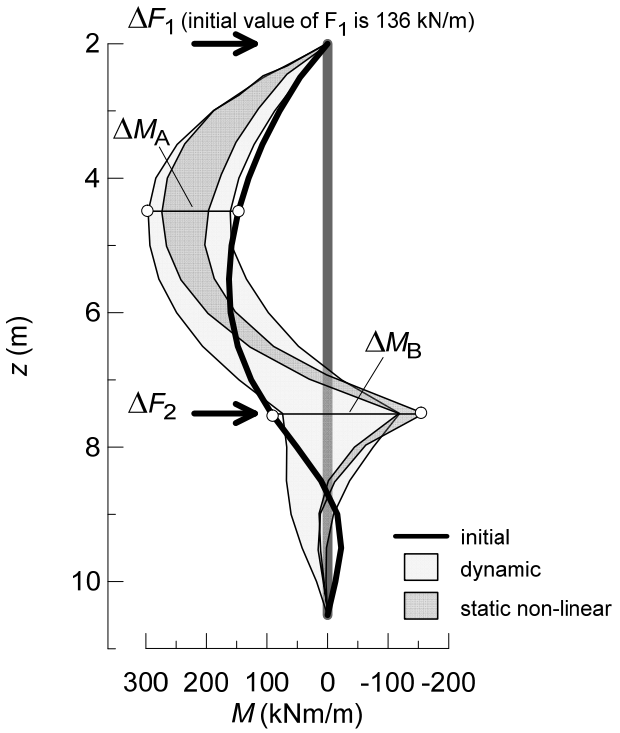

Figure 5 – Profiles of the bending moment (the effect of seismic actions refer to the Tolmezzo record).

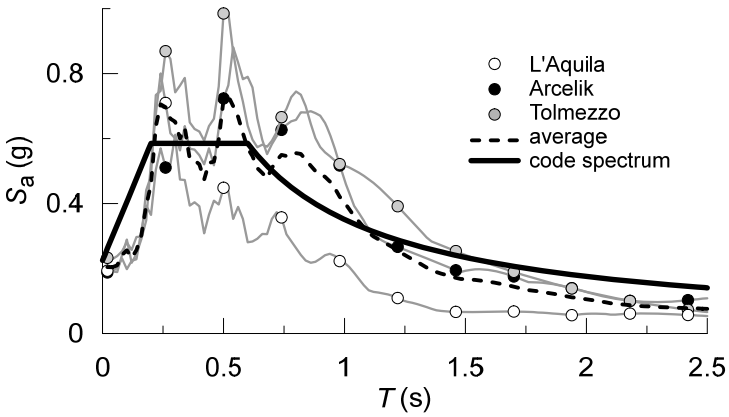

Figure 6 – Elastic response spectra obtained from the ground response analysis and interpolated with a code spectrum. The spectra are plotted for a damping ratio ξ = 5 %.

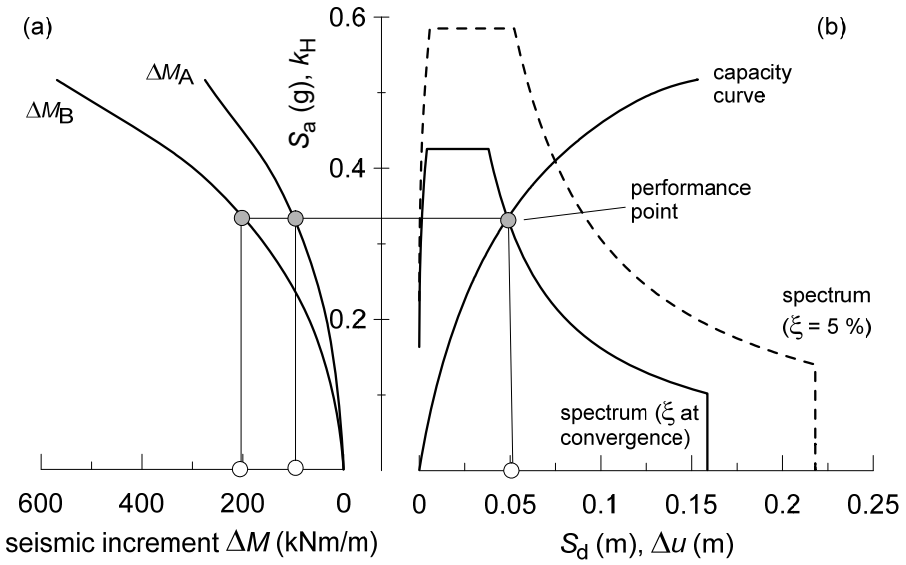

Figure 7 – Implementation of the design method representing the seismic demand through a code spectrum. (a) relationship between the seismic coefficient and the increment of bending moment at two locations; (c) capacity and demand in the AD plane.

The overall comparison between the results of the simplified method and the dynamic analyses is depicted in Figure 8. This is a bi-logarithmic plot that is used to perform two separate comparisons:

- The results of each dynamic analysis is compared with the corresponding implementation of the static push-over analysis (as in Figure 3). This comparison is represented by the open symbols.
- The average values of each quantity obtained with the dynamic analyses is compared with the implementation of the static push-over analysis in which the seismic demand is expressed by the code spectrum, as in Figure 7 (denoted by the full symbols). This latter is intended to be the actual practical application of the method.

The quantities included in the comparison are, in addition to the seismic displacement u of the top of the walls, the seismic increments of the bending moments ΔM_A and ΔM_B in the wall at a depth of 4.5 and 7.5 m, respectively, and the variation of the prop forces ΔF_1 and ΔF_2 in the two props (for the bottom prop the variation ΔF_2 is equal to the axial force, because it is installed at the end of the excavation phase). As shown in Figure 5, for each

analysis type, the seismic increments of bending moments are evaluated as the maximum differences from the initial static condition.

Figure 8 also includes the 1:1 line and some lines of equal error. Inspection of Figure 8 reveals that, although individual errors can be significant, the average error of the proposed method is quite acceptable, being smaller than 50 % for most of the scrutiny quantities, and always on the safe side. An exception are the seismic forces in the lower prop, that are somewhat overestimated by the simplified method.

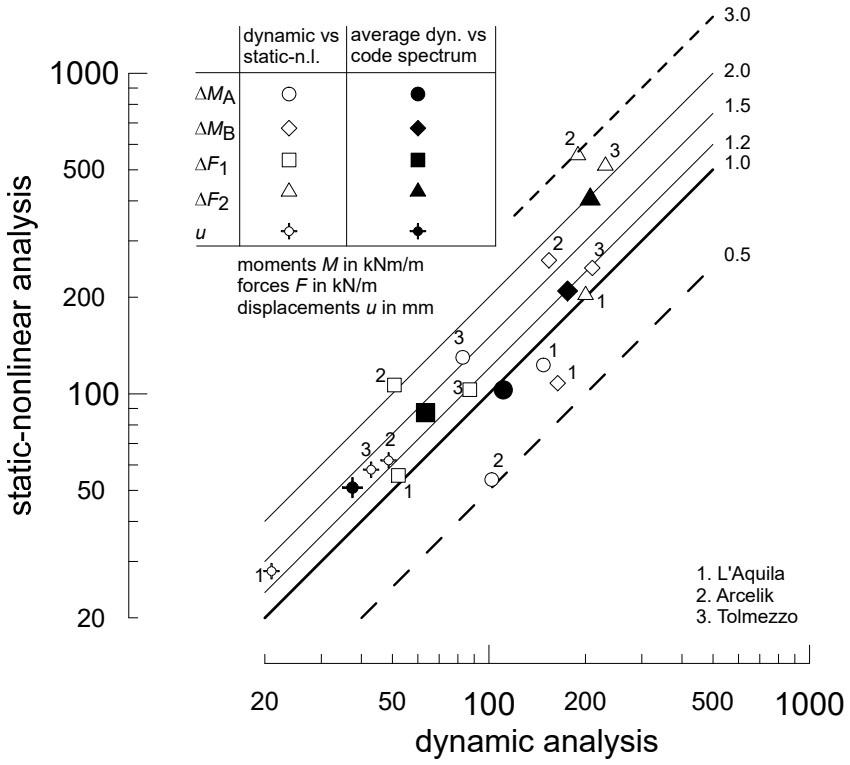

Figure 8 – Overall comparison of the results obtained with the dynamic analyses and with the simplified method.

5. DISCUSSION AND CONCLUSIONS

The seismic design of multi-propped retaining structures is based on the maximum transient increment of the internal forces in the structural members. Therefore, the seismic demand can be effectively expressed by a design elastic spectrum, collecting the maximum instantaneous seismic actions expected at a given site for a given return period, provided that it accounts for the local ground response. The seismic capacity can be

expressed by a capacity curve, that can be obtained by an immediate extension of the non-linear soil-structure interaction analysis carried out to design the structure against the static actions. The superposition of demand and capacity onto the AD plane provides, after a few iterations, a performance point that describes with a sufficient accuracy the seismic response of the system.

The design method proposed in this paper employs a seismic action that is derived as the equivalent acceleration obtained in a free-field ground response analysis from equation (1). In the absence of a ground response analysis, the equivalent spectral acceleration and displacements can obtained correcting the code spectrum, relative to actions at the ground surface, with a factor related to the ratio of the wall height to the dominant wavelength of the seismic action (for instance the one developed by the Author of the present paper and included in Annex A of FprEN 1998-5 2023, which for the present case would assume a value of about 0.96).

It its present form, the method is sufficiently robust for most applicative cases. Its main merit is the ability to cope with the many different construction sequences and static schemes that characterise the type of retaining structures at hand, and to provide an immediate appreciation of the dynamic response of the system. It is instructive to note from both Figure 3 and Figure 7 that the ordinate of the performance point is significantly larger than the PGA, which is the first spectral ordinate. This means that by neglecting the deformability of the soil-structure system the internal forces in the structural members would by largely underestimated.

This can also be demonstrated by observing that the ratio of the coordinate of the performance point provides an estimation of the natural vibration period corresponding to the secant stiffness of the system:

$$\frac{gk_{\mathrm{H}}}{u} = \frac{S_{\mathrm{a}}}{S_{\mathrm{d}}} = \left(\frac{2\pi}{T_0}\right)^2$$
$$T_0 = 2\pi\sqrt{\frac{u}{gk_{\mathrm{H}}}} = 2\pi\sqrt{\frac{0.05}{0.33\times g}} \approx 0.8 \text{ s} \tag{4}$$

and noting that a period of 0.8 s is well within the range of the frequency content of any seismic action: in practice the dynamic response of the system can never be neglected.

On the other hand, from both figures 3 and 7 it is evident that the non-linearity of the system is always engaged by the seismic action. Therefore, any linear assumption for the system would be quite arbitrary and would produce unreliable results.

Acknowledgement

The Author wishes to express his gratitude to Mr Alessandro Fortuna for carrying out a large part of the numerical analyses presented in this paper.

REFERENCES

Brandenberg S.J., Mylonakis G., and Stewart J.P. 2015. Kinematic framework for evaluating seismic earth pressures on retaining walls. Journal of Geotechnical and Geoenvironmental Engineering, 141, No 7 doi: /10.1061/(ASCE)GT.1943-5606.0001312.

Callisto, L. 2023. From "De la pression des terres et des revêtements" to the seismic analysis of retaining structures. Rev. Fr. Geotech. 2023, 175, 6 doi: /10.1051/geotech/2023008.

Callisto, L. 2019. On the seismic design of displacing earth retaining systems. In: Earthquake geotechnical engineering for protection and development of environment and constructions. In: Proceedings of the 7th international conference on earthquake geotechnical engineering. Associazione Geotecnica Italiana, Rome, pp 239–255

Callisto, L. 2014. Capacity design of embedded retaining structures. Géotechnique 64(3): 204–214. doi: /10.1680/geot.13.P.091

Callisto, L., & Soccodato, F.M. 2010. Seismic design of flexible cantilevered retaining walls. Journal of Geotechnical and Geoenvironmental Engineering 136(2): 344–354. doi:/10.1061/(ASCE)GT.1943-5606.0000216

Cecconi, M., Pane, V. & Vecchietti, A. Seismic displacement-based design of embedded retaining structures. Bull Earthquake Eng 13, 1979–2001 (2015). https://doi.org/10.1007/s10518-014-9708-8

European Committee for Standardization (CEN). (2003). Eurocode 8: Design of structures for earthquake resistance—Part 1: General rules, seismic actions and rules for buildings. EN 1998-1,CEN, Brussels,Belgium.

European Committee for Standardization (CEN). (2023a). Eurocode 8: Design of structures for earthquake resistance—Part 5: Geotechnical aspects, foundations, retaining and underground structures FprEN 1998-5,CEN, Brussels,Belgium.

European Committee for Standardization (CEN). (2023b). Eurocode 8: Design of structures for earthquake resistance— Part 1-1: General rules and seismic action FprEN 1998-1-1,CEN, Brussels,Belgium.

FEMA 440 (2005). Improvement of nonlinear static seismic analysis procedures. AppliedTechnology Council (ATC-55 Project). Redwood City, California, 2005.

Fortuna, A. (2020). Seismic behaviour of propped retaining walls (in Italian). Master thesis, Sapienza University of Rome.

Freeman, S.A. (1998) Development and use of capacity spectrum method. In: Proceedings of the 6th US National Conference on Earhquake Engineering. Seattle, Washington, USA

Itasca (2011). FLAC fast lagrangian analysis of continua v. 7.0. User's manual, Itasca Consulting Group, Minneapolis, Minn.

Laguardia, R. Gallese, D. Gigliotti, R. and Callisto L.. A non-linear static approach for the prediction of earthquake-induced deformation of geotechnical systems. Bulletin of Earthquake Engineering, 18(15):6607–6627, 2020. ISSN 1573-1456. doi: 10.1007/s10518-020-00949-2.

Lorusso C. 2017. Prediciton of earthquake-induced displacement in flexible retaining structures (in Italian). MSc Thesis, Sapienza Università di Roma. (in Italian).

Masing, G. (1926). "Eigenspannungen und Verfertigung bim Messing. Proc., 2nd Int. Congress on Applied Mechanics, Zurich, Switzerland.

NTC (Norme tecniche per le costruzioni). Decreto Ministero Infrastrutture e Trasporti 17 gennaio 2018. (In Italian).

Seed, H. B., and Idriss, I. M. (1979). Soil moduli and damping factors for dynamic analysis. Rep. No. EERC 70-10, University of Califor-nia, Berkeley, Calif.

Seed, H.B. and Martin G.R. (1966). The seismic coefficient in earth dam design. Journal of Soil Mechanics and Foundation Division, ASCE, 92 (3), 25-58.

Wood, J. H. (1973). Earthquake induced soil pressures on structures. Rep. No. Earthquake Engineering Research Laboratory (EERL) 73-05, California Institute of Technology, Pasadena, CA.

Younan, A.H. and Veletsos A.S. (2000). Dynamic response of flexible retaining walls. Earthquake Engineering and Structural Dynamics. 29, 1815-1844. Doi: /10.1002/1096-9845(200012)29:12%3C1815::AID-EQE993%3E3.0.CO;2-Z

FIGURE CAPTIONS

Figure 1 – Layout of the case study and finite-difference grid, with an indication of the different boundary conditions used for the static and the dynamic calculations.

Figure 2 – Elastic response spectra of the acceleration time histories used as seismic actions, plotted for a damping ratio ξ = 5 %.

Figure 3 – Tolmezzo record. (a), (b) static push-over analysis: (b) analysis in the AD plane; (a) increment in bending moment obtained from the static push-over analysis. (c), (d) time-histories of the increment in bending moment and of the wall displacement obtained from the dynamic analysis.

Figure 4 – (a) velocity vectors and (b) deformed grid at the attainment of the critical acceleration.

Figure 5 – Profiles of the bending moment (the effect of seismic actions refer to the Tolmezzo record).

Figure 6 – Elastic response spectra obtained from the ground response analysis and interpolated with a code spectrum. The spectra are plotted for a damping ratio ξ = 5 %.

Figure 7 – Implementation of the design method representing the seismic demand through a code spectrum. (a) relationship between the seismic coefficient and the increment of bending moment at two locations; (c) capacity and demand in the AD plane.

Figure 8 – Overall comparison of the results obtained with the dynamic analyses and with the simplified method.